

Depth-based Localization for Robotic Peg-in-Tube Assembly

Arun Dayal Udai¹, Ravi Prakash Joshi² and Subir Kumar Saha³

Abstract—Peg-in-Tube assembly stands ahead of a more common benchmark task for industrial assembly, i.e., ‘peg-in-hole’. The robot can easily be deceived to detect the actual hole while performing a ‘peg-in-tube’ task as the tube has a surrounding pocket that cannot support the peg. The paper presents a thorough geometrical analysis of the ‘peg-in-tube’ assembly process, and proposes a novel algorithm based on depth measurements of peg center to perform ‘peg-in-tube’ task. The results are demonstrated on a KUKA KR5 Arc industrial robot with a chamferless cylindrical peg and a tube having clearance of 0.10 mm.

I. INTRODUCTION

Peg-in-tube forms the superset of industrial assembly task where the possibility of finding the target hole is obscured. This is because there exists a surrounding pocket which may be mistaken with the actual hole where the part is to be inserted. The existing well researched peg-in-hole task forms a special case of peg-in-tube task where the outer radius of the tube is infinity. Many such cases exist in the industry which may be pronounced as peg-in-tube task. For example, inserting a piston into the cylinder liner, inserting a plunger into a cylindrical fuel pump barrel, putting cylindrical fuel pellets into a tube in a nuclear power plant, fitting a shaft into a circular bush, etc. Most of the existing peg-in-hole strategies are inappropriate to search the hole location on a tube in its current form. Some of them can be modified beneficially to be used for peg-in-tube task as well. There are primarily two different approaches to the hole search problem. The first one uses the robot’s end-effector position, whereas the second one uses a force/torque sensor fitted at the robot’s end-effector.

A 6-axis force/torque sensor data was used to precisely estimate the shape and location of the peg with respect to the hole [1]. Relying entirely on force sensor data is not worthwhile in a typical industrial environment where the force sensor data is proven to have a very high noise [2]. These noise may be attributed to the mechanical vibration of the work floor, electrical noise, electromagnetic radiations, etc. For any two surfaces in contact and in relative motion, the measured contact force will depend largely on their surface finish and the force controller gains. Moreover, if the surface stiffness is high, a small relative displacement due to

vibration will cause a high value of noise in the sensed force. Same applies to any force/moment based method for hole detection, which will be more evident through an experiment described later in this paper as well.

A blind search strategy for localization by generating a depth map of the tilted peg center from the hole surface, and applying a particle filter to locate the hole was proposed by [3]. This method has the potential to be used for ‘peg-in-tube’ case as well, but the depth map is required to be regenerated if the dimensions of the peg or the hole changes. Generating a new map is time consuming if it is prepared online using the robot holding the peg, and complicated if it is generated offline using simulations based on analytical methods. Moreover, an analytical depth map may not be realized for actual localization if the environmental constraints like, system compliance, surface finish, etc., are not taken into account for creating the depth map. Due to the presence of pockets around the actual hole, finding a unique hole location on a tube by plunging the peg for a lesser number of times is ruled out, as this will give rise to multiple solutions. Moreover, plunging the peg for a larger number of times will increase the insertion time. A strategy for high-precision assembly in a semi-structured environment based on vision and force control was demonstrated by [4]. Detecting the pellet pose using machine vision suffers from calibration errors, blurred view for objects that are close by, improper illumination, noise due to the background environment, etc. Also, the time required to assemble with spiral search used by [4] depends on the initial offset of the peg from the peg center. A set of environment-independent search strategies was proposed by [5], where a neural-network based strategy based on moments and descent of the peg into the hole was generalized for tilted peg. Such optimization techniques are suited well for offline simulations but it may prove to be non-realistic for a real time insertion. Moreover, the hybrid force/position control as suggested by [5] cannot be applied to a position controlled industrial robot. A high speed assembly of peg and chamfered holes using learning was demonstrated by [6] using joint torque controlled robots. Such robots, however are not used in the industry where the robots are required to perform precision tasks with heavy loads.

Therefore, a blind search technique is needed that can efficiently eliminate the possibility of peg being dropped outside the tube, provided it is brought sufficiently near to the hole using existing automation, to say, using a vision system.

This paper proposes a hole search method which measures the depth of the tilted peg center from the top surface of the

*The reported research was carried out under a sponsored project funded by BARC/BRNS, Mumbai, India.

¹Arun Dayal Udai is a Research scholar in the Department of Mechanical Engineering, IIT Delhi. arun_udai@yahoo.com

²Ravi Prakash Joshi is one of the Senior Research Fellows in the Department of Mechanical Engineering, IIT Delhi. ravi2008joshi@gmail.com

³Subir Kumar Saha is a professor in the Department of Mechanical Engineering, IIT Delhi, India. saha@mech.iitd.ac.in

tube while the peg rotates about the axis perpendicular to the tube's top surface by one full revolution. The profile of this depth was used to find the direction of the hole.

Note here that the positioning repeatability of an industrial robot is typically in the range of $100 \mu m$. For example, the KUKA KR5 Arc robot used in this work has $\pm 0.10 mm$, i.e. $100 \mu m$ positioning repeatability, whereas most of the assembly tolerance is in the order of few tens of microns [1]. Position and orientation error can cause jamming and wedging during insertion. An active force control with passive joint compliance based on current limiting, as proposed by the authors in [7], is expected to solve this problem by accommodating any minute alignment error during insertion. However, the current work assumes the peg is aligned with the tube using any suitable method like [8]. This is demonstrated with the current experimental setup used for the validation of the proposed peg-in-tube algorithm. To simplify the problems presented above, the paper uncovers the geometrical aspects and the practical considerations that are required to be understood before dealing with chamferless cylindrical peg-in-tube task. Secondly, the paper proposes a novel algorithm to tackle 'peg-in-tube' task. Experimental results presented here shows the viability of the proposed algorithm.

The remainder of this paper is organized as follows: Section II lays down the geometrical foundations required to be developed to analyze the details of the proposed peg-in-tube task. Section III discusses the proposed algorithm for the 'peg-in-tube' task. Section IV investigates the effectiveness of the proposed algorithm through experimental results. Finally, Section V gives the conclusions.

II. GEOMETRICAL ANALYSIS OF PEG-IN-TUBE CONTACT

The proposed search procedure involves rotating a tilted peg about the axis which is perpendicular to the tube's top surface while the peg maintains a constant contact with the tube. Thus, the peg moves in a cone with a half-angle of the vertex equals to the amount of the tilt angle θ , as shown in Fig. 1.

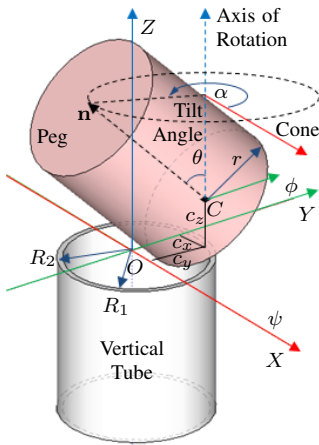


Fig. 1: A tilted peg in contact with the tube.

This section will investigate the geometrical aspects of

such contact cases and will extract the required peg center depth c_z from the tube's top surface, as shown in Fig. 1. This depth information was utilized later to find the hole direction. A tilted peg when lies outside the hole with an offset (c_x, c_y, c_z) , can make contact with the tube in four different states. They are shown in Fig. 2(a – d). There are two other states in which the peg can make contact with the hole. Firstly, when the curved surface of the peg comes in contact with the tube's inner rim, as shown in Fig. 2(e), and secondly, when the peg's bottom cap comes in contact with the tube's inner curved surface, as shown in Fig. 2(f). Latter two cases do not arise during rotation of the tilted peg, which was done during search procedure adapted here in this paper. Hence it is not analyzed anywhere. It may be noticed that the peg-in-tube process has two additional contact cases compared to a peg-in-hole process [9]. They are 1) when the outer rim of the tube and rim of the peg's bottom cap comes in contact, as shown in Fig. 2(c); 2) when the peg's bottom cap face comes in contact with the tube's outer edge as shown in Fig. 2(d).

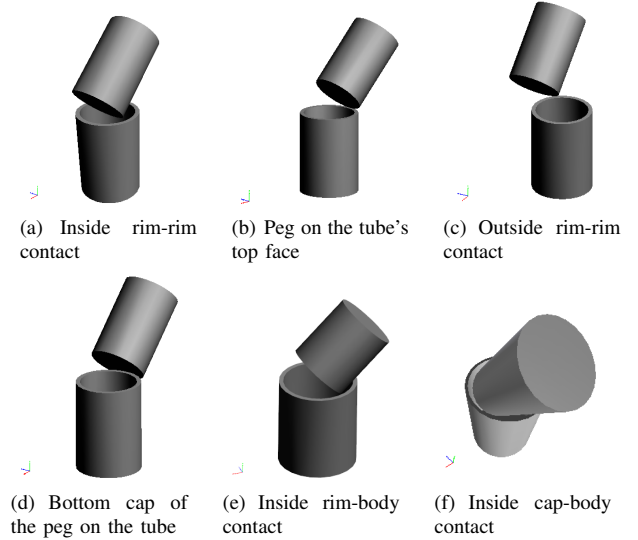


Fig. 2: States of contact for Peg-in-Tube

A. Parametric modeling of the peg and tube

In this section, we define the peg and the tube surfaces, and their edges before we proceed to establish the conditions of peg lying inside, outside or on the tube. The bottom of the peg was defined by a parametric equation for a 3-Dimensional circle. This is given by

$$\mathbf{p} = \mathbf{c} + \mathbf{u}r \cos \beta + \mathbf{v}r \sin \beta \quad (1)$$

where \mathbf{u} and \mathbf{v} are the unit vectors that lie on the peg's bottom face and perpendicular to the vector $\mathbf{n} \equiv \mathbf{u} \times \mathbf{v}$, as shown in Fig. 3. The radius of the peg is r , and \mathbf{c} is the position vector of the peg's bottom center. The parametric angle β is measured about \mathbf{n} with respect to \mathbf{u} . For each $0 \leq \beta \leq 2\pi$, $P(x, y)$ represents the peg's bottom rim. Any composite tilt about X and Y axes was obtained by applying

the transformation as

$$\mathbf{u}' = \mathbf{Q}_x \mathbf{Q}_y \mathbf{u} \text{ and } \mathbf{v}' = \mathbf{Q}_x \mathbf{Q}_y \mathbf{v} \quad (2)$$

where \mathbf{Q}_x and \mathbf{Q}_y are the 3×3 rotation matrices about X and Y axes, respectively. To start with $\mathbf{u} = [1 \ 0 \ 0]$ and $\mathbf{v} = [0 \ 1 \ 0]$ were taken, such that $\mathbf{n} = [0 \ 0 \ 1]$. Thereafter, the rotations were applied so as to obtain the required tilt angle. Now, for any point $P(x, y)$ having position vector \mathbf{p} at the bottom-end cap of the peg, the condition $(\mathbf{p} - \mathbf{c}) \cdot \mathbf{n} = 0$ holds true as the vector $(\mathbf{p} - \mathbf{c})$ lies on the plane for which the normal $\mathbf{n} = [n_x \ n_y \ n_z]$ which passes through $\mathbf{c} = [c_x \ c_y \ c_z]$. This condition is essentially the vector expression for representing the bottom-end cap of the peg. This may be written in scalar form as

$$n_x(x - c_x) + n_y(y - c_y) + n_z(z - c_z) = 0 \quad (3)$$

With this any contact with the peg's bottom surface or the edge can be geometrically explained. For that, the parametric equations for the tube hole are given next as

$$x = R_1 \cos(\xi) \text{ and } y = R_1 \sin(\xi) \quad (4)$$

where $0 \leq \xi \leq 2\pi$ and R_1 is the inner radius of the tube, as shown in Fig. 1. Similarly, the outer edge of the tube with radius is R_2 .

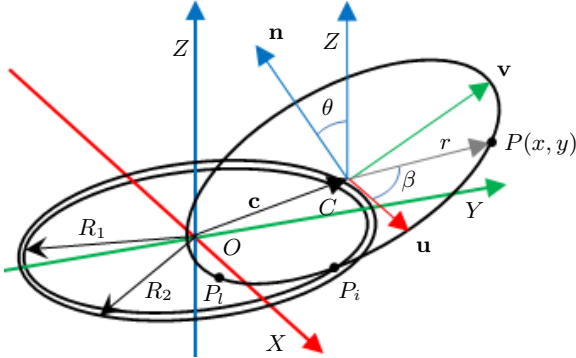


Fig. 3: A 3-Dimensional circle.

B. The rotating tilted peg

Let us assume that the peg has a small tilt angle of θ and rotates about the vertical axis by an angle α , as shown in Fig. 1. Then the tilt angle about global X and Y axes given by ψ and ϕ , respectively, may be expressed as

$$\psi = \arcsin(\sin \alpha \sin \theta) \text{ and } \phi = \arcsin(\cos \alpha \sin \theta) \quad (5)$$

where $0 \leq \alpha \leq 2\pi$. The projection of the peg's bottom cap forms a rotated ellipse and it constitutes an important aspect to identify the point of contact. The modified equation of the standard ellipse E to express the projected base of the peg may be expressed as

$$E = \frac{(\tilde{x})^2}{a^2} + \frac{(\tilde{y})^2}{b^2} - 1 \quad (6)$$

where $a = r$ and $b = r \cos \theta$ are the major and minor axes, respectively. Moreover, \tilde{x} and \tilde{y} are given by

$$\begin{bmatrix} \tilde{x} \\ \tilde{y} \end{bmatrix} = \begin{bmatrix} \cos \alpha & \sin \alpha \\ -\sin \alpha & \cos \alpha \end{bmatrix} \begin{bmatrix} x - c_x \\ y - c_y \end{bmatrix} \quad (7)$$

The state of the peg may now be completely defined by θ , α and the offset $\mathbf{c} = [c_x \ c_y \ c_z]$ from the tube center which was taken as origin \mathbf{O} here. The lowermost point of the peg $P_l = (x_l, y_l, z_l)$ was given by the 3D circle equation (1), at $\beta = \alpha$. The location of P_l will enable us to determine the possible point of contact. The point of intersection of the projected peg's base and the tube $P_i = (x_i, y_i, 0)$ was obtained by solving E of (4) and (6). The potential point of contact is the P_i which is nearest to P_l . The possible location of P_i for a sample state of the peg is shown in Fig. 3.

C. Cases of peg and tube in contact

The cases discussed here completely defines the rotation of the tilted peg about a vertical axis passing through the peg's bottom center, while the peg also maintains a constant contact with the tube during the rotation. The state of the peg for each case was examined individually and the depth information was extracted accordingly. They are explained next.

1) *Peg lies inside the tube:* The projection of lowermost point of the peg P_l lies within the tube's inner circle, i.e., the hole, as shown in Fig. 2(a). This can be assured by checking, if the condition $x^2 + y^2 - R_1^2 < 0$ is true for the point P_l . The point of intersection of the projected ellipse E and tube's inner rim P_i that corresponds to the point of contact (the one which is nearer to P_l) satisfies the equation of the plane (3). Thus the depth c_z may be calculated from (3) as

$$c_z = \frac{1}{n_z} [n_x(x_i - c_x) + n_y(y_i - c_y)] \quad (8)$$

2) *Peg lies on the tube:* The lowermost point lies between the inner and outer circular rims of the tube. Thus, P_l makes $x^2 + y^2 - R_1^2 \geq 0$ and $x^2 + y^2 - R_2^2 \leq 0$, and the depth c_z from Fig. 3 may be given by

$$c_z = r \sin \theta \quad (9)$$

This is shown in Fig. 2(b).

3) *Peg lies outside the tube:* The lowermost point lies outside the outer circular rim of the tube. Thus, P_l makes $x^2 + y^2 - R_2^2 > 0$. In this case the peg may have a rim-rim contact case, as shown in Fig. 2(c) or rim-face contact case, as shown in Fig. 2(d). In the case when the peg's cap comes in contact with the outer tube rim, the line joining the center of the tube O to the point of contact $P_t = (x_t, y_t, 0)$ becomes parallel to the projected normal of the cap's plane. This gives rise to the simultaneous conditions

$$\frac{x_t}{y_t} = \frac{n_x}{n_y} \text{ and } x_t^2 + y_t^2 = R_2^2 \quad (10)$$

Solving which, we get the point $P_t = (x_t, y_t, 0)$ as

$$\begin{aligned} x_t &= \text{sign}(n_x) \sqrt{\frac{R_2^2}{1 + (n_y/n_x)^2}} \\ y_t &= \text{sign}(n_y) \frac{n_y}{n_x} x_t \end{aligned} \quad (11)$$

For, $n_x = 0, x_t = 0$. Hence, the two sub-cases may be further investigated as

- Rim-rim contact: P_t lies outside the ellipse E and makes $E > 0$, as shown in Fig. 2(c). Thus, P_i i.e., the point of intersection of E and tube's outer circle, lies on the peg's bottom rim and it satisfies the cap's plane equation (3). Hence, from (3)

$$c_z = \frac{1}{n_z} [n_x(x_i - c_x) + n_y(y_i - c_y)] \quad (12)$$

- Rim-face contact: P_t lies inside the ellipse E , i.e., the projected bottom cap of the peg, as shown in Fig. 2(d). Thus for P_t lying on the peg's cap plane, P_t makes $E < 0$. On substituting $P_t = [x_t \ y_t \ 0]$ in (3) we get

$$c_z = \frac{1}{n_z} [n_x(x_t - c_x) + n_y(y_t - c_y)] \quad (13)$$

4) *Curved surface contact*: With relatively large offset and a small tilt angle, the curved surface contact is kept out and hence its analysis is not included here. However, for the sake of completeness of the peg model it is briefly being included here. Any point \mathbf{q} on the peg's curved surface may be assumed to be an equidistant point from the cylinder's axis. This may be represented as a point-line distance in 3D [10] as

$$r = \frac{|\mathbf{n} \times (\mathbf{c} - \mathbf{q})|}{|\mathbf{n}|} \quad (14)$$

With the scalar equation (14) and conditions for the end caps boundaries, i.e., the plane equations (3), one can detect any point falling inside the peg surfaces.

III. THE PROPOSED ALGORITHM

The algorithm makes use of the fact that, when a tilted peg attains a two point contact during rotation, the projection of the peg axis represents the direction of the hole and the peg center reaches the minimum depth c_z . Thus, the method of finding the hole direction involves rotating the tilted peg about the axis which is perpendicular to the tube's top plane and passes through the peg center. The peg rotates by one complete revolution and finally finds the angle α for which the peg lowers to the minimum depth c_z measured along the axis of rotation. This corresponds to the hole direction. The contact with the tube was maintained using the force control algorithm as discussed in [7]. Such a hole search process with a tube will have two minima in the depth profile. The proposed algorithm eliminates the minimum value which corresponds to the direction that will lead to peg being moved in the opposite direction to that of the actual hole. Algorithm III.1 demonstrates how an analytical depth profile can be generated using the conditions discussed in section II-C. This was used later in section IV as shown in

Fig. 5, which shows the analytical depth profile for a peg radius of $r = 9.42\text{mm}$, tilt angle of $\theta = 7.5^\circ$, tube radius $R_1 = 9.7\text{mm}$ and $R_2 = 12.65\text{mm}$.

Algorithm III.1: GENERATEDDEPTHPROFILE(θ, \mathbf{c})

comment: Generate the depth profile

$r, R_1, R_2 \leftarrow$ **by definition**

for $\alpha \leftarrow 0$ **to** 360

do {	}	$\psi, \phi \leftarrow$ From (5)
		$\mathbf{Q}_x \leftarrow$ <i>function_of</i> (ψ)
		$\mathbf{Q}_y \leftarrow$ <i>function_of</i> (ϕ)
		$\mathbf{u} \leftarrow \mathbf{Q}_x \mathbf{Q}_y \mathbf{u}, \mathbf{v} \leftarrow \mathbf{Q}_x \mathbf{Q}_y \mathbf{v}$
		$\mathbf{n} \leftarrow \mathbf{u} \times \mathbf{v}$
		$P_l \leftarrow$ <i>function_of</i> (α) From (1)
		if $x_l^2 + y_l^2 - R_1^2 < 0$
		then {
		Solve (4) and (6) for P_i
		$c_z \leftarrow$ from (8)
else if {		
$(x_l^2 + y_l^2 - R_1^2 > 0)$ and		
$(x_l^2 + y_l^2 - R_2^2 < 0)$		
then { $c_z \leftarrow r \sin(\theta)$ from (9)		
else if $x_l^2 + y_l^2 - R_2^2 > 0$		
{		
$P_t \leftarrow$ From (11)		
if $E < 0$ for P_t . From (6)		
then { $c_z \leftarrow$ from (13)		
{		
Solve (4) with R_2		
and (6) for P_i		
$P_i \leftarrow P_i$ nearest to P_l		
$c_z \leftarrow$ from (12)		
}		
save α, c_z		

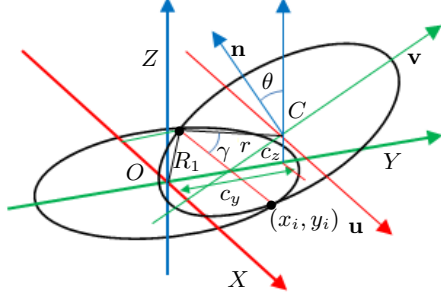
The two minima which can be observed in Fig. 5 lies opposite to each other, i.e., 180° apart at 90° and 270° . The inner tube hole will form a narrow depression in the profile such that the lowest point is non-differentiable. The profile with the wider opening and continuous at minima is formed when the flat bottom part of the peg rolls on the outer periphery of the tube. As the offset of the peg increases from the center of the hole, the depth realized for inner tilt which directs to the hole direction decreases and the depth for outer tilt which directs opposite to the direction of the hole increases. Hole direction can be safely detected just by checking the maximum depth location, until the offset for which the depth due to inner tilt is greater than for the outer tilt. This is derived next.

A. Maximum offset for safe hole detection

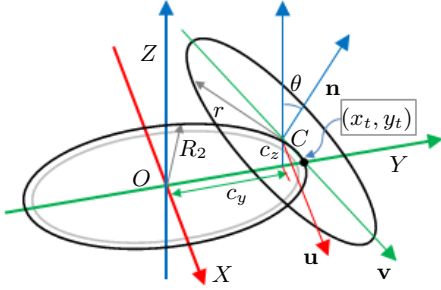
Figure 4(a) shows a two point contact case when the depth c_z is minimum for the inner tilt. Figure 4(b) on the other hand shows the outer rim contact where the depth c_z is again minimum. This is in the case of outer tilt. Let the offset be c_y measured along Y -axis, i.e., for $c_x = 0$, where the depth due to inner tilt is same as that of the outer tilt with the peg

having tilt angle θ . The conditions for both the cases are as follows:

$$\begin{aligned} \text{a) Inner tilt} & \begin{cases} n_x = 0, n_y = -\sin \theta, n_z = \cos \theta \\ \text{Contact point: } x_i, y_i \end{cases} \\ \text{b) Outer tilt} & \begin{cases} n_x = 0, n_y = \sin \theta, n_z = \cos \theta \\ \text{Contact point: } x_t = 0, y_t = R_2, z_t = 0. \end{cases} \end{aligned} \quad (15)$$



(a) Two point rim-rim contact during inner tilt.



(b) Single point rim-face contact during outer tilt.

Fig. 4: Instances of peg-in-tube contacts having same depth.

Substituting the cases (15a) and (15b) in (8) and (13) respectively, we get

$$\begin{aligned} \text{a) } c_z &= \frac{1}{\cos \theta} [\sin \theta (R_2 - c_y)] \\ \text{b) } c_z &= \frac{1}{\cos \theta} [-\sin \theta (y_i - c_y)] \end{aligned} \quad (16)$$

Using trigonometrical relations in Fig. 4(a), we get

$$r \sin \gamma = \frac{c_z}{\sin \theta} \quad \text{and} \quad \cos \gamma = \frac{x_i}{r} \quad (17)$$

The point of contact (x_i, y_i) can now be obtained as

$$\begin{aligned} \text{From (17), } x_i &= r \sqrt{1 - \frac{c_z^2}{r^2 \sin^2 \theta}} \\ \text{and from (16b), } y_i &= c_y - \frac{c_z}{\sin \theta} \cos \theta \end{aligned} \quad (18)$$

Substituting (x_i, y_i) from (18) in the condition $x_i^2 + y_i^2 = R_1^2$, we get

$$r^2 + c_y^2 - c_z^2 - \frac{2c_y c_z}{\tan \theta} = R_1^2 \quad (19)$$

Substituting c_z from (16a), a quadratic equation in c_y was obtained as

$$(3 - \tan^2 \theta) c_y^2 - 2R_2(1 - \tan^2 \theta) c_y + (r^2 - R_2^2 \tan^2 \theta - R_1^2) = 0 \quad (20)$$

Solving (20) for a realistic case with positive solution, c_y was obtained. This offset is expected to assist one to choose a suitable precision of the sensing system to approach the tube, i.e., a vision system, a laser range sensor, or a 3D-point cloud scanner etc.

B. Detecting hole direction and insertion

Once the rotation was completed for $0 \leq \alpha \leq 2\pi$, the value of α corresponding to the least depth α_{min} was recorded. The peg was then made vertical, i.e., with tilt angle $\theta = 0$, and a constant desired contact force was maintained. The direction of the hole was obtained as

$$\Delta x = k_1 \cos \alpha_{min} \quad \text{and} \quad \Delta y = k_1 \sin \alpha_{min} \quad (21)$$

Or, by using (5) as

$$\Delta x = k_2 \sin \psi_{min} \quad \text{and} \quad \Delta y = k_2 \sin \phi_{min} \quad (22)$$

where k_1 and k_2 are the constants of proportionality. Now, the peg was advanced with continuous small displacements of Δx and Δy along X and Y , respectively, until it senses a reduced reaction force due to the presence of the hole. The robot was now stopped and the peg was inserted gradually into the hole. Note that the values of k_1 or k_2 directly affect the advancing velocity towards the hole. Their value depend on the clearance between the tube and the hole. They were kept small in our experiments due to the possibility of skipping of the peg over the hole.

C. Algorithm for Implementation

In order to use the proposed algorithm the steps given in Algorithm III.2 was used with a KUKA KR5 Arc robot. It was assumed that the peg is to be brought near to the top of the tube using any suitable system, for example, a vision system. The robot provides the end-effector coordinates (X, Y, Z) in its base frame, where Z is vertically up and parallel to the tube axis. The peg was tilted, and lowered using a force control mode, i.e., if the peg senses any contact it would maintain the desired force $F_{desired}$. The small decrement in the robot's end-effector coordinate Z , i.e., Δz , should be kept very small as establishing a contact at high speed will give rise to an undesired thrust that can damage the surface of tube or peg. While the peg is rotated for $0 \leq \alpha \leq 360^\circ$ the algorithm updates the minimum Z value, i.e., Z_{min} with the current Z if it is lower than the existing Z_{min} . It also sets the variable α_{min} to the value of α corresponding to Z_{min} . Once the rotation is complete the peg was made vertical by setting the tilt angle θ to 0. The peg was then moved towards the hole using (22) till it finds the hole, where the peg senses a reduced reaction force F_z than the desired force, or the peg gets into the hole by a small distance d . The peg was then lowered gradually into the hole.

Algorithm III.2: PEGINTUBE(θ , c)

comment: Algorithm for implementation

START: Peg over the tube

$Z_{min} \leftarrow Z$

$\theta \leftarrow$ tilt angle

while $F_z \leq F_{desired}$

do $Z \leftarrow Z - \Delta z$

for $\alpha \leftarrow 0$ to 360°

do $\left\{ \begin{array}{l} \psi, \phi \leftarrow \text{From (5)} \\ \text{if } Z < Z_{min} \\ \text{then } \left\{ \begin{array}{l} Z_{min} \leftarrow Z \\ \alpha_{min} \leftarrow \alpha \end{array} \right. \end{array} \right.$

$\theta \leftarrow 0$

$\Delta x, \Delta y \leftarrow$ From (22)

while $F_z > F_{desired}$ **OR** $Z > Z_{min} - d$

do $\left\{ \begin{array}{l} X \leftarrow X + \Delta x \\ Y \leftarrow Y + \Delta y \end{array} \right.$

END: Insert the peg

IV. EXPERIMENTAL RESULTS AND DISCUSSIONS

A KUKA KR5 Arc industrial robot was used to validate the proposed peg-in-tube algorithm. The parameters for the tube and for the peg were same as given in section III. A monocular camera system was used to bring the peg directly over the tube. However, its discussion is excluded as it will divert the focus of this paper. The end-effector was mounted with a six component Force/Torque sensor manufactured by SCHUNK of type Delta, SI-165-15. In order to measure the vertical depth during the hole search procedure as discussed in section III, we relied on the in-built forward kinematics of KUKA KR5 Arc robot.

Figure. 5 shows the depth profiles obtained experimentally and analytically peg radius of $r = 9.42mm$, tilt angle of $\theta = 7.5^\circ$, tube radii $R_1 = 9.7mm$ and $R_2 = 12.65mm$, and an offset of $c = (-7.53, -7.2, 0)mm$. A close match of the depth profiles validates the proposed Algorithm III.1. The difference in the depth profiles is mainly due to experimental procedure. Some of them are discussed in the following subsections.

A. Force/Torque Sensor and DAQ

The force/torque sensor used for the experiment was of high bandwidth with $495N$ along vertical Z -direction and a low sensor resolution of $1/16N$ using a 16-bit Data Acquisition (DAQ) system. The DAQ was used to pass the analog voltages of 6 strain gauges to the controller. These data were filtered using a real-time low pass fourth-order Butterworth filter with cut-off frequency of $40Hz$. The sampling frequency was $83.33Hz$. The force data was generated by multiplying the 6-dimensional vector of voltages with the 6×6 sensor calibration matrix. The resulting force data had a typical noise of $\pm 0.15N$.

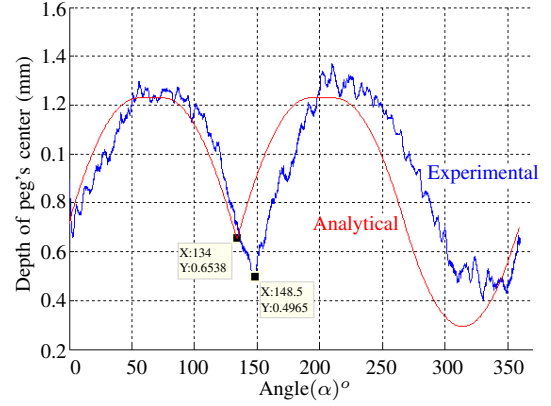


Fig. 5: Theoretical vs. analytical depths.

B. Effect of peg size and clearance

The bigger peg will definitely accommodate more placement error, i.e., the offset, in order to have a safe hole direction detection as per (20). However, in order to study the effect of peg sizes, two different pegs were analyzed. Figure 6 shows the analytical depth profile for two different pegs of radii $9.42mm$ and $24.0mm$ when the peg center lies on the tube rim, i.e., with offset equal to the mean tube radius $c_x = (R_1 + R_2)/2$ and $c_y = 0$. The peg and tube had a radial clearance of $0.28mm$ for both the cases.

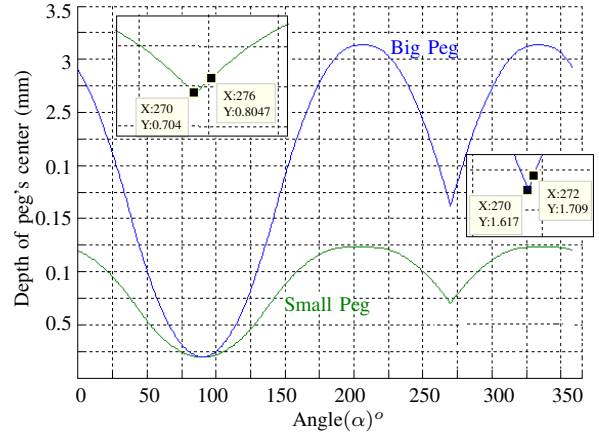


Fig. 6: Depth profiles for peg radii $9.42mm$ and $28.0mm$.

It was observed that the differences in depths of two minimums are $0.526mm$ and $1.516mm$, respectively, for smaller and bigger pegs. These differences are required to be distinguished clearly using depth observations made by robot's sensory system to estimate the correct hole direction. It becomes even more difficult when the depth data are accompanied with the noise as well. This limits the minimum size of the peg which can be handled using the proposed algorithm with the setup used in this paper. The authors could successfully insert peg of diameter $18mm$ with 95% success rate (tested with 40 pegs) using the existing setup. For smaller pegs and smaller offset a blind spiral search [4] may be used instead.

It may be observed in Fig. 6 that an error in depth

measurement by $0.1mm$ will cause corresponding hole direction error of 6° and 2° for smaller and the bigger pegs, respectively. This quantifies the hole direction error for a particular depth measurement error. If the smaller peg proceeds with directional error of 6° with offset amounting to the peg radius, it will reach to $0.984mm$ away from the actual hole. In the case of bigger peg, 2° directional error will lead to $0.977mm$ hole position error. Thus, a system with an error of $0.1mm$ in depth measurement may not successfully perform peg insertion with a peg and tube having clearance of $1mm$ or less.

C. Other sources of error

Apart from force sensing and displacement measurement errors, this section lists the additional sources of errors that limit the performance of peg-in-tube process. Following points may be noted while designing the peg-in-tube assembly systems:

- Passive compliance of the gripper system allows unaccounted motion of the peg-tip.
- Assuming the tube's top face perfectly flat is just an ideal case. Peg and tube axes alignment is also required which may be done using [8].
- Poor surface finish of the rolling surfaces of peg and tube creates force/displacement noise.
- Two-finger gripper cannot hold the peg firm enough to restrict small linear and angular motions of the peg with respect to the robot's end-effector during contact.
- Due to inaccurate tool calibration, the peg never makes pure rolling during search procedure. Any slipping on the edge will create noise.
- At high speed force control response is poor which may cause undue contact forces or a loss of contact. However, with 10% Point-to-Point speed of KUKA KR5 Arc robot four consecutive pegs were inserted in 22.5 seconds. This included picking of peg from a fixed location, bringing the peg directly over the tube, searching for the hole, and finally inserting the peg, for each of the peg.
- An industrial floor with high vibration may also lead to reduced performance.

D. Force vs. Depth based hole detection

In order to have a comparison between the depth based localization proposed here and the force based localization, both the depth and the forces/moments were recorded during the rotation of the peg. The radii of the tube was $23.62mm$, while the inner and outer radii of the tube was $24.5mm$ and $28mm$, respectively. The tilt angle was set to 7.5° . The offset was kept so as to have just one minima, i.e., the peg's outer rim falls on the tube's flat face. Figure 7(a) shows the polar plot for the variation of the depth with respect to angle α . The variation of vertical force can be seen in Fig. 7(b). The coherence of force plot with the depth plot where the minimum depth may be observed is notable. A sharp rise in force was observed that can be effectively used

for hole direction estimation. This surge force was created when the peg starts rising up after the two point contact, i.e., the minimum depth. The hole direction due to force profile is consistent to that of the depth profile, i.e., at $\alpha = 218.4^\circ$. The force data shows the filtered data in dark, along with the actual data acquired through the force sensor. With the unfiltered data it is difficult to figure out the surge due to the hole in realtime, whereas with filtered data a lag was observed that might again lead to a wrong hole direction. One may estimate the lag with proper knowledge of the filter parameters. It may however be inferred with the data that is shown in Fig. 7 that the depth data provides a better localization of the hole direction. A similar surge in moments was also observed in moments at 214.8° , i.e., at the hole direction. This is not shown here due to space constraints.

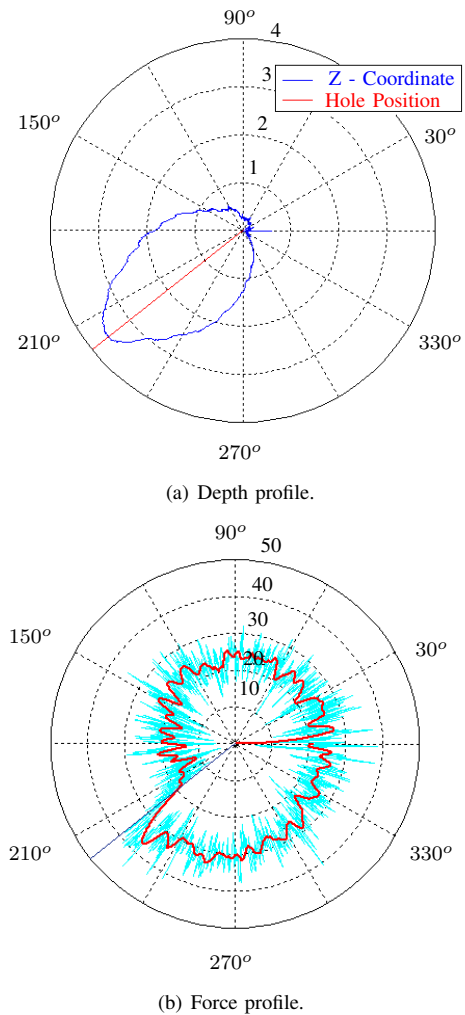


Fig. 7: Profiles for the peg of radius $23.62mm$.

There are various checks which one may devise in order to encounter any failed attempt and incorrect placement of the peg. For example, one may check if the peg moves more than its radius while moving towards the hole. Accordingly, the robot algorithm may be designed to search the hole again. Similarly, if the peg gets into the hole without touching

the tube surface, the peg may be released without starting the search procedure. The system may also be programmed to remember the hole location once it is located using the proposed search technique to repeatedly insert the peg at the same hole location. Again as a check, one may lower the peg using a *guarded move*, i.e., by continuously checking the contact force, and if the peg hits the tube surface the search process may be redone.

V. CONCLUSIONS

This paper presents a depth-based approach to localize the hole position of a tube for a peg-in-tube process. Peg-in-tube was addressed as an illustration for wider set of assembly processes which are encountered in any industrial assembly task. The proposed algorithm can handle a wide range of pegs and tubes combinations without modifying the code or re-calibrating the robot's end-effector tool, provided the peg is held at a same height from its base. The hole position with offset as high as the peg radius can be detected reliably. The proposed method minimizes the effect of error due to external force/moment data acquisition system and relies on the existing forward kinematics that exists in any industrial robot in order to find the depth and thereby the hole. While the proposed method addresses only the positional errors, the procedure makes use of an indigenous active/passive force control algorithm, reported differently, to accommodate any small misalignment encountered during the insertion phase. With relatively high tolerance, the insertion becomes a self-guided assembly.

This paper presented an in-depth geometrical analysis of the peg-in-tube process. The cases of contact discussed in section II-C may be used to generate an analytical depth map and can be used for localization using method proposed by [3]. The challenges, however, remain the same for any depth-based localization technique. These cases may also be used for generating simulations of any cylindrical peg and tube contacts or its assembly process. Finally, the proposed algorithm for peg-in-tube assembly was tested on a KUKA KR5 Arc industrial robot and was found to be more reliable than any other blind search algorithm under similar condition.

ACKNOWLEDGMENTS

The authors sincerely acknowledge the technical inputs given by Mr. Kamal Sharma from BARC, Mumbai, and members of Programme for Autonomous Robotics (PAR) Lab., IIT Delhi, India.

REFERENCES

- [1] Y. Kim, B. Kim, and J. Song, "Hole detection algorithm for square peg-in-hole using force-based shape recognition," in *8th IEEE Int. Conf. on Automation Science and Engineering*, Seoul, Korea, August 2012, pp. 1074–1079.
- [2] S. Katsura, Y. Matsumoto, and K. Ohnishi, "Modeling of force sensing and validation of disturbance observer for force control," *IEEE Trans. on Ind. Elect.*, vol. 54, no. 1, pp. 530–538, 2007.
- [3] S. R. Chhatpar and M. S. Branicky, "Particle filtering for localization and in robotic assemblies with position uncertainty," in *IEEE/RSJ Int. Conf. on Intelligent Robots and Systems*, 2005, pp. 3610–3617.

- [4] H. Chen, G. Zhang, H. Zhang, and T. A. Fuhlbrigge, "Integrated robotic system for high precision assembly in a semi-structured environment," *Assembly Automation*, vol. 27, no. 3, pp. 247–252, 2007.
- [5] K. Sharma, V. Shirwalkar, and P. K. Pal, "Intelligent and environment-independent peg-in-hole search strategies," in *IEEE Int. Conf. on Control, Automation, Robotics and Embedded Systems*, Noida, India, 2013.
- [6] B. Nemeč, F. Abu-Dakka, B. Ridge, A. Ude, J. Jorgensen, T. Savarimuthu, J. Jouffroy, H. Petersen, and N. Kruger, "Transfer of assembly operations to new workpiece poses by adaptation to the desired force profile," in *16th International Conference on Advanced Robotics (ICAR 2013)*, 2013, pp. 1–7.
- [7] A. D. Udai, A. A. Hayat, and S. K. Saha, "Parallel active/passive force control of industrial robots with joint compliance," in *IEEE/RSJ Int. Conf. on Intelligent Robots and Systems*, Chicago, Illinois, 2014.
- [8] S. Huang, K. Murakami, Y. Yamakawa, T. Senoo, and M. Ishikawa, "Fast peg-and-hole alignment using visual compliance," in *IEEE/RSJ International Conference on Intelligent Robots and Systems*, Tokyo, Japan, 2008, pp. 286–292.
- [9] J. Zhou, N. D. Georganas, E. M. Petriu, X. Shen, and F. Marlic, "Modelling contact forces for 3D interactive peg-in-hole virtual reality operations," in *IEEE Instrumentation and Measurement Technology Conference*, British Columbia, Canada, 2008.
- [10] E. W. Weisstein. Point-Line Distance–3-Dimensional. <http://mathworld.wolfram.com/Point-LineDistance3-Dimensional.html>. [Online; accessed 01-September-2014].